ELSEVIER

International Journal of Mass Spectrometry 220 (2002) 399–418

International Journal of Mass Spectrometry

www.elsevier.com/locate/ijms

Expanded theory for the resolving power of a linear ion mobility spectrometer

Glenn E. Spangler

Technispan LLC, 1133C Greenwood Road, Pikesville, MD 21208-3625, USA

Received 14 February 2002; accepted 21 July 2002

Abstract

An expanded theory for the resolving power of a linear ion mobility spectrometer (IMS) is derived. By definition, the resolving power is directly proportional to the total drift time for the ion through the drift tube divided by the full-width-at-half-height (FWHH) of the observed ion mobility peak. Two approaches to theoretically estimating these two parameters are possible, depending on the operating parameters of the IMS cell. The drift time is given by the first moment of the IMS response. If the electric fields (assumed uniform) are equal in both the shutter/aperture and aperture/collector region, the FWHH is given by a difference in error functions. If the electric fields (again assumed uniform) are not equal, the FWHH is given by the second central moment of the IMS response and can only be known to within a multiplicative factor. The effectiveness of these two approaches is demonstrated using IMS data from the published literature.

The additional peak broadening often observed in a linear IMS has several possible sources. One depends on the construction of the cell and the parallelism (or lack thereof) that might exist between the aperture grid and ion collector. Another depends on electric fields used to bias the cell. If the electric field in the aperture/collector region is less than in the shutter/aperture region, peak broadening occurs. Induction effects in the aperture/collector region not only shorten drift times, but also create diffusion-like broadening of the peak. Shortening the distance between the aperture grid and ion collector, or using a higher electric field in that region, minimizes induction effects. Drift time calibration requires adjustments for induction effects. (Int J Mass Spectrom 220 (2002) 399–418)
© 2002 Elsevier Science B.V. All rights reserved.

Keywords: Ion mobility spectrometry (IMS); Expectation values (Drift time); Moment analysis (Peak width); Induced current; Collision cross section; Theory

1. Introduction

Ion mobility spectrometry (IMS) is an ionization technique used in combination with a drift tube to identify ions. While IMS shares with mass spectrometry the ability to separate ions, the two techniques are different. Mass spectrometry identifies ions based on observed charge-to-mass ratios, while IMS identifies ions based on drift times (or ion mobility). Although the mobility of an ion is proportional to the ratio of the charge to the square root of the reduced mass of the ion, it is also inversely proportional to the collision cross-section. The collisions impede and scatter the motion of the ion to degrade the resolving power of the instrument. The ability of IMS to separate peaks as required to identify ions has been the subject of intensive investigation [1].

E-mail: gspan@aol.com

1387-3806/02/$ – see front matter © 2002 Elsevier Science B.V. All rights reserved.
PII S1387-3806(02)00841-2

The ion separation capabilities of IMS are quantified using either the *resolving power* or the *peak-to-peak resolution* formalisms. Both formalisms are taken from gas chromatography where the resolving power corresponds to the square root of the number of theoretical plates [2], and the peak-to-peak resolution is a more practical assessment of peak separation. For IMS, the resolving power R is given by [3,4]

$$R = \frac{t_d}{\omega_h} \tag{1}$$

where t_d is the drift time and ω_h is the temporal full-width-at-half-height (FWHH) for the mobility peak. Similarly, the peak-to-peak resolution R_{pp} is given by [5,6]

$$R_{pp} = 2\left(\frac{t_{d2} - t_{d1}}{\omega_{b1} + \omega_{b2}}\right) \tag{2}$$

where t_{d1} and t_{d2} are drift times for two neighboring ion mobility peaks, and ω_{b1} and ω_{b2} are their temporal full-widths measured at the baseline of the IMS signature. Since the peak-width-at-half-height is more easily measured than the peak-width-at-baseline, Eq. (2) is sometimes written as

$$R_{pp} = \frac{2(t_{d2} - t_{d1})}{1.7(\omega_{h2} - \omega_{h1})} \tag{3}$$

where the peak shape is assumed to be Gaussian. An obvious difference between Eqs. (1) and (2) is that only a single peak is needed to obtain data on R, while two neighboring peaks are needed to obtain data on R_{pp}.

In the absence of reactions with time constants on the order of, or longer than, the drift time, IMS typically produces Gaussian peaks (assuming a narrow pulse width is applied to the shutter grid). For this situation, $t_{d2} - t_{d1}$ is proportional to $t_{d1} \cong t_{d2} \equiv t_d$, and $\omega_{h1} \cong \omega_{h2} = \omega_h$, so that $R = \alpha_R R_{pp}$ where α_R is a constant proportional to the ratio between $t_{d2} - t_{d1}$ and t_d. When comparing the performance of two instruments, R is generally preferred over R_{pp} due to the arbitrariness of α_R. On the other hand, R_{pp} is well suited to assess conditions that lead to unit resolution ($R_{pp} = 1$), baseline resolved peaks ($R_{pp} = 1.5$), or the minimum acceptable resolution ($1.75 < R_{pp} < 2.0$) [7,8].

Since simple mobility theory relates the drift time for an ion to the length, l_d, and voltage, V, applied to the drift tube, through

$$t_d = \frac{l_d^2}{KV} \tag{4}$$

where K ($cm^2\,V^{-1}\,s^{-1}$) is the mobility of the ion, Eq. (1) can be rewritten as

$$R = \frac{l_d^2}{\omega_h KV} \tag{5}$$

Eq. (5) indicates that the resolving power of an IMS is increased (improved) by increasing the length of the drift tube, even though the dependence of R on l_d is not explicitly stated due to the dependence of ω_h on l_d. Similarly, Eq. (5) also indicates that the resolving power of an IMS is decreased (degraded) by increasing the drift potential. This second statement is incorrect since the FWHH, ω_h, also depends on V that causes R to "increase" with increasing V. For more details on these relationships, the reader is refered to the work of Siems et al. [4].

Using a sum of variances approach similar to that applied by Knox and McLaren [9] and Gasper et al. [10] in gas chromatography, Spangler and Collins wrote down an expression for the FWHH [11]

$$\omega_h^2 = t_{diff}^2 + t_g^2 \tag{6}$$

where t_g is the initial width of the gate pulse applied to the shutter grid and t_{diff} is the temporal width-at-half-height of a Gaussian peak created by diffusion broadening of a narrow ion packet as it drifts through the drift tube [12]. Expanding on this definition, Siems et al. fitted their data to [4]

$$\omega_h^2 = \alpha\frac{Tt_d^2}{V} + \beta t_g^2 + \gamma \tag{7}$$

where T is the temperature of the drift gas and α, β and γ are parameters that adjust the diffusion, gate width and offset contributions, respectively. Although Revercomb and Mason included Eq. (6) in their classic review of IMS [13], it has not yet been supported by rigorous computations derived, for example, from the continuity equation first written down by Moseley

et al. and later applied by Spangler and Collins, to the study of peak shape in IMS [11,14].

Experiences with fitting Eqs. (6) and (7) to experimental data have shown that Eq. (6) consistently underestimates measured FWHHs [11], and larger than expected α and β parameters (γ should be unnecessary) are needed to describe the resolving power [4]. Various reasons have been given for this. They include:

- Contributions from transverse diffusion lengthening the flight time for the ion through the drift tube.
- Electrostatic repulsion of neighboring ions in the drifting ion cloud [11,15].
- Enhanced longitudinal diffusion due to elevated ion energies (Townsend energy factor) [11].
- Distortions in the pulsed electric field (voltage) created near the shutter grid [16].
- Delayed ion arrivals due to encounters with an inhomogeneous electric field generated near the segmented guard rings of the IMS cell [4].
- Distortions created by a non-uniform field between the aperture grid and ion collector.
- Inadequate response time for the electrometer.

Except for the last three, each of these explanations has been discredited for one reason or another.

For example, Schummers et al. (sighting the work of Moseley et al. [17]) observed that the transverse diffusion coefficient affects only the amplitude of the ion mobility peak, and not its shape [18]; an observation consistent with the two-temperature model for IMS [19]. Spangler and Eiceman et al. observed that ion concentrations were not high enough in the drifting ion cloud to indicate significant electrostatic repulsion effects [20–22]. Siems et al. noted that the Townsend energy factor must be near 1 (not 2.7 as proposed by Spangler and Collins [11]), because the ions are near thermal energies while drifting through the drift tube [4]. Albritton et al. regarded the radial inhomogeneities in the drift field to be negligible, reaching 1% at two-thirds the inside radius of the drift tube, and deteriorating rapidly beyond that due to the exponential nature of the Bessel function [23]. Spangler et al. observed no significant improvement in resolution when using uniformly inlaid ceramic resistor tubes vs. stacked rings for their drift tubes [6,11], but other design features their IMS cell may have masked results. Wu et al. were able to improve the resolving power (with loss of signal) of their stack-ring IMS cell by decreasing the ion transmission area of their aperture grid [24]. Finally, work with photo-etched parallel plane shutter grids has eliminated the shutter grid as a significant source of distortions [25].

The objective of the present work was to revisit the theoretical issues associated with the resolving power of IMS. The desire was to throw additional light on, if not eliminate, the vagaries described above. The starting point was the continuity equation [26], and the ending point was an analytical expression for the FWHH. Since the work was performed assuming a uniform electric field within the drift tube, issues associated with non-uniform drift fields were not addressed.

2. Elementary theory

2.1. Basic concepts

Before deriving the theory, it is necessary to conceptualize the processes that occur as an ion travels from the shutter grid to the ion collector of an IMS. Fig. 1 shows a cloud of positive ions approaching the ion collector that is additionally coupled to the virtual input ground of an electrometer amplifier. The top illustration shows that as the ion cloud approaches the collector, the electrostatic field radiated by the ions induces a current flow in the electrometer circuit, causing an image charge ($-\delta$) to develop on the ion collector. The net result is that the electrometer senses an arriving ion cloud, but not yet the direct ion current. The bottom illustration shows that when the direct ion current actually hits the collector plate, it again causes current to flow in the electrometer circuit. The direction of current flow through the feedback resistor is the same for both the induced and direct current flows. Thus, the two current flows are additive as the ion cloud approaches and hits the collector plate.

Fig. 2 shows another configuration where an aperture grid is placed between the approaching ion cloud

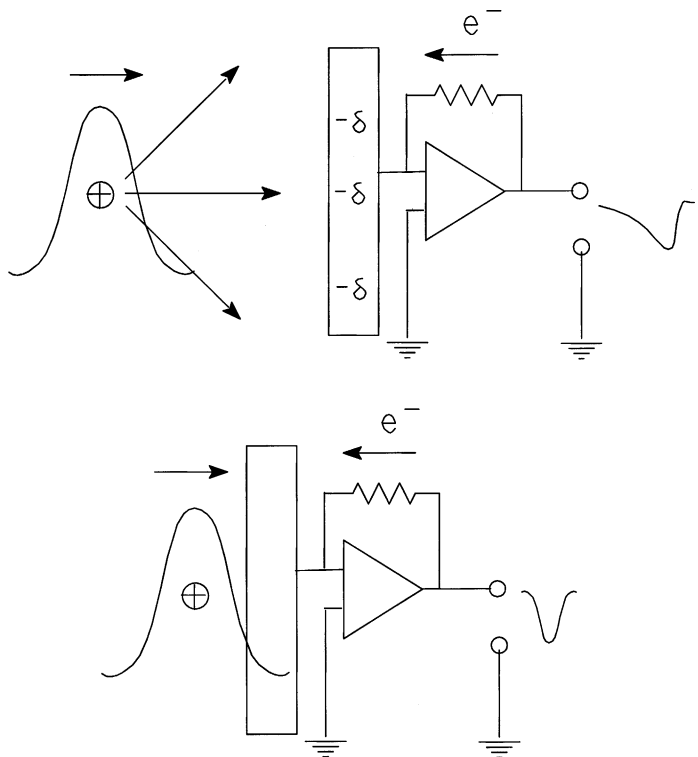

Fig. 1. An illustration for an ion cloud approaching and then hitting the ion collector of an ion mobility spectrometer. The top figure demonstrates that the ionic charge induces surface charge on the ion collector, and this surface charge is supplied by electron flow through the feedback resistor of the electrometer. The bottom figure demonstrates that electron flow again occurs through the feedback resistor as the ion cloud hits the ion collector, and that the electron flow is in the same direction as the induced current flow.

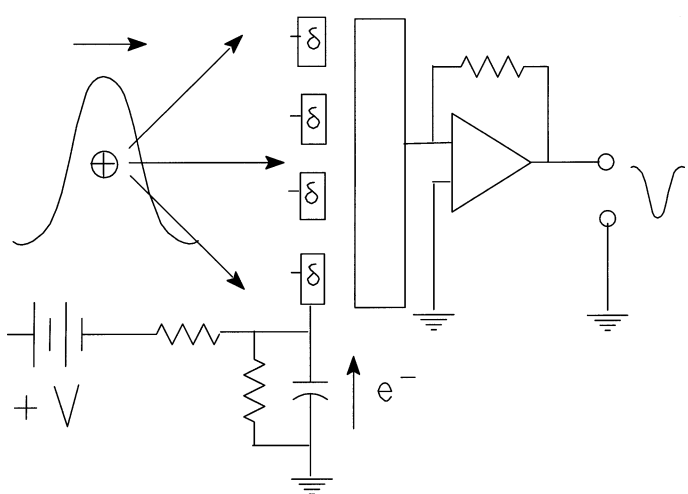

Fig. 2. An illustration showing how an aperture grid interposed between an approaching ion cloud and ion collector shields the ion collector from induced charge. A ballast capacitor is added to serve as a ready source of electrons that can flow into the aperture grid.

and ion collector [27]. The function of the aperture grid is to intercept the electrostatic field radiated by the approaching ion cloud so that it no longer induces current flow in the electrometer circuit. To avoid the aperture grid acting as a capacitor in combination with the ion collector to differentiate the arriving ion signal, a "large" ballast capacitor is added to the aperture grid to drain the current away from the collector. That is, the ballast capacitor is a high pass filter (or sink) to ground. When all these conditions are met, the electrometer circuit registers only the direct current arriving at the ion collector.

Unfortunately, the condition that the electrometer registers only the arrival of direct ion current can never be really met. There must always be a region of finite distance between the aperture grid and ion collector, and when an ion cloud of any significant extent migrates through the region, induced and direct ion current flows are registered by the electrometer circuit. Consequently, any theory that addresses the resolving power of an IMS must take into account influences from both the induced and direct current flows.

2.2. Basic theory

Spangler and Collins showed that the on-axis ($r = 0$) concentration $n(0, z, t)$ for a migrating ion cloud in a cylindrical IMS is given by

$$n(0,z,t) = \mp\frac{n_0}{2}\exp[(\langle\alpha\rangle - k_1^-)t]\left[1-\exp\left(-\frac{r_0^2}{4D_T t}\right)\right] \times\left[\mathrm{erf}\left(\frac{z-v_d t}{2\sqrt{D_L t}}\right)-\mathrm{erf}\left(\frac{z-v_d t \pm v_d t_g}{2\sqrt{D_L t}}\right)\right] \quad (8)$$

where t_g is the pulse width applied to the shutter grid, z the location of the cloud along the longitudinal axis of the drift tube ($z = 0$ at the shutter grid), t the time measured from the gate pulse, n_0 the initial ion concentration introduced into the drift tube at $t = z = 0$, v_d the drift velocity for the ions, D_L and D_T the longitudinal and transverse diffusion coefficients, r_0 the internal radius of the cylindrical drift tube, $\langle\alpha\rangle$ and k_1^- are the rate constants associated with the creation and annihilation of ions as they drift through the drift tube, and $+$ or $-$ is selected depending on the slope of the trigger pulse used to synchronize data acquisition [11]. If losses due to ion conversion, recombination or transverse diffusion are negligible, Eq. (8) becomes

$$n(0,z,t) = \mp\frac{n_0}{2}\left[\mathrm{erf}\left(\frac{z-v_d t}{2\sqrt{D_L t}}\right)-\mathrm{erf}\left(\frac{z-v_d t \pm v_d t_g}{2\sqrt{D_L t}}\right)\right] \quad (9)$$

Fig. 3 shows a plot of Eq. (9) at $z = l_d$ (l_d is the length of the drift tube) with the individual contributions of the error functions to the resultant Gaussian peak indicated.

For the purposes of this paper, Eq. (9) will be assumed to contain all the information needed to describe the concentration profile of a migrating ion cloud, and hence the shape of an ion mobility peak arriving at the ion collector ($z = l_d, t = t_d$). If losses due to ion conversion, recombination or transverse diffusion are important, modifications to the theory will be necessary.

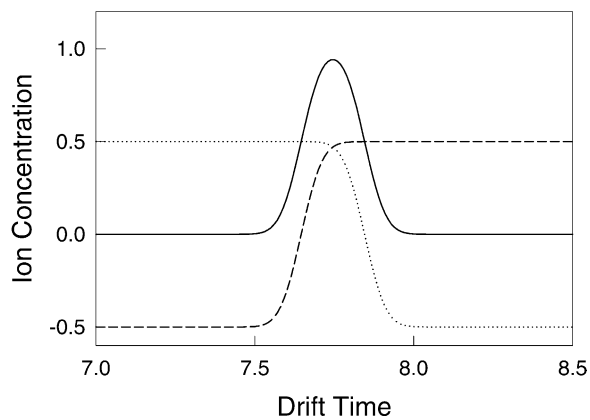

Fig. 3. A MathCAD printout showing how an ion mobility peak can be constructed using a difference in error functions. The dotted curve is given by $n_1(0, l_d, t) = 0.5[\mathrm{erf}((l_d - v_d t)/(2\sqrt{D_L t}))]$, the dashed curve is given by $n_2(0, l_d, t) = -0.5[\mathrm{erf}((l_d - v_d t - v_d t_g)/(2\sqrt{D_L t}))]$ and the solid curve is $n_1(t) + n_2(t)$, or the ion mobility peak.

By setting the first derivative of Eq. (9) with respect to time equal to 0 and solving for t_{max}, the location for the highest concentration of the migrating ion cloud is found. With the exponentials arising from the differentiation expanded to the second order and z assumed approximately equal to $v_d t$, the result is

$$t_{max} \simeq \frac{z}{v_d} \pm \frac{t_g}{2} + \frac{D_L}{v_d^2} + \frac{12D_L^2 + v_d^4 t_g^2}{16 z v_d^3} \quad (10)$$

This result can be compared to the expectation value for the drift time calculated from the first moment

$$\langle t \rangle = \frac{\int_{-\infty}^{\infty} tn(0,z,t)\,dt}{\int_{-\infty}^{\infty} n(0,z,t)\,dt} = \frac{z}{v_d} \pm \frac{t_g}{2} \quad (11)$$

using the mathematical procedures described in Appendix B. The difference between Eqs. (10) and (11) are the additional terms containing D_L in Eq. (10). Since these terms typically add no more than 0.2 μs to the calculated drift time (compared to 50–500 μs for t_g), $\langle t \rangle$ is approximately equal to t_{max}, and Eq. (11) provides a convenient way to estimate t_{max}. Since Urquijo et al. [28] draw similar conclusions for $zv_d/2D_L > 100$, the essential equivalence of $\langle t \rangle$ and t_{max} will be assumed in this paper.

When Eq. (11) is substituted back into Eq. (9), the maximum ion concentration arriving at the ion collector is

$$n_{max}(0,z,t) \simeq n_0 \left[\mathrm{erf}\left(\frac{v_d t_g}{4\sqrt{D_L t_{max}}} \right) \right] \quad (12)$$

The FWHH for the ion concentration is derived by setting half of Eq. (12) equal to Eq. (9), and evaluating the combination at $z = l_d$ and $t = t_{max} \simeq t_d \pm (t_g/2) \pm (\omega_h/2)$. The result is

$$\mathrm{erf}\left(\frac{v_d t_g}{4\sqrt{D_L t_{max}}} \right) = \mathrm{erf}\left(\frac{v_d t_g + v_d \omega_h}{4\sqrt{D_L t_{max}}} \right) + \mathrm{erf}\left(\frac{v_d t_g - v_d \omega_h}{4\sqrt{D_L t_{max}}} \right) \quad (13)$$

where ω_h is the FWHH. Within the limits of the approximations applied, Eq. (13) describes reasonably well the relationship between the FWHH and the operating parameters of an IMS cell.

3. Advanced theory

The simple theory just described applies only to the flow of direct ion current through a non-compartmentalized drift tube. The drift tube for a real IMS cell, however, is compartmentalized with two drift regions, one before and one after the aperture grid. As the ion cloud migrates toward the aperture grid, the ion collector is shielded from the ionic charge by the aperture grid. As the ion cloud passes through the aperture grid, the electrometer circuit senses the arriving ionic charge either as direct or induced current flow. Acknowledging that the two regions are unique and peculiar, a special notation is needed to comprehensively describe ion motion through each. The formalism of Spangler will be used for this purpose [25].

3.1. Direct current flow

According to Spangler, the time spent by the ion as it travels from the shutter grid to the ion collector is $t_{sa} + t_{ac}$, where t_{sa} is the time spent in the shutter/aperture region, and t_{ac} is the time spent in the aperture/collector region. While Spangler assumed that t_{sa} and t_{ac} were the absolute drift times through the two regions, this requirement can be relaxed, allowing t_{sa} and t_{ac} to become two statistically independent variables. For example, in the shutter/aperture region, Eq. (9) indicates that the ion concentration arriving at the aperture grid is

$$n(0, d_{sa}, t_{sa}) = \mp \frac{n_0}{2} \left[\mathrm{erf}\left(\frac{z - v_{sa} t_{sa}}{2\sqrt{D_{Lsa} t_{sa}}} \right) - \mathrm{erf}\left(\frac{z - v_{sa} t_{sa} \pm v_{sa} t_g}{2\sqrt{D_{Lsa} t_{sa}}} \right) \right] \Bigg|_{z=d_{sa}} \quad (14)$$

where d_{sa} is the electrode separation between the shutter and aperture grids, and D_{Lsa} and v_{sa} are the diffusion coefficient and drift velocity for the ions in the shutter/aperture region. When a narrow gate pulse is applied to the shutter grid (i.e., $t_g \ll t_{sa}$), Eq. (14) describes a Gaussian distribution of ions arriving at the aperture grid as t_{sa} increases with time. When the gate

pulse is wide, the peak shape broadens, and assumes features more like the initial square pulse applied to the shutter grid.

In the aperture grid/collector region, the ion concentration approaching the ion collector is calculated by convoluting Eq. (14) with a Gaussian distribution to yield [29]

$$
\begin{aligned}
&n(0, z, t_{sa} + t_{ac}) \\
&= \mp \frac{n_0 T_i}{4\sqrt{\pi D_{Lac} t_{ac}}} \int_{-\infty}^{\infty} \left\{ \exp\left[-\frac{(z - z' - v_{ac} t_{ac})^2}{4 D_{Lac} t_{ac}} \right] \right. \\
&\quad \left. \times \left[\operatorname{erf}\left(\frac{z' - v_{sa} t_{sa}}{2\sqrt{D_{Lsa} t_{sa}}} \right) - \operatorname{erf}\left(\frac{z' v_{sa} t_{sa} \pm v_{sa} t_g}{2\sqrt{D_{Lsa} t_{sa}}} \right) \right] \right\} \mathrm{d}z' \\
&= \mp \frac{n_0 T_i}{2} \left[\operatorname{erf}\left(\frac{z - v_{sa} t_{sa} - v_{ac} t_{ac}}{2\sqrt{D_{Lsa} t_{sa} + D_{Lac} t_{ac}}} \right) \right. \\
&\quad \left. - \operatorname{erf}\left(\frac{z - v_{sa} t_{sa} - v_{ac} t_{ac} \pm v_{sa} t_g}{2\sqrt{D_{Lsa} t_{sa} + D_{Lac} t_{ac}}} \right) \right] \qquad (15)
\end{aligned}
$$

where D_{Lac} and v_{ac} are the diffusion coefficient and drift velocity for the ions in the aperture/collector region, and T_i is a transmission factor for the aperture grid [30]. Again an ion cloud with a Gaussian distribution is described that evolves into a rectangular distribution as t_g increases. Thus, the direct ion current density, J_{direct}, of ions arriving and hitting the collector plate is

$$
\begin{aligned}
&J_{direct} \\
&= \mp \frac{n_0 T_i q v_{ac}}{2} \left[\operatorname{erf}\left(\frac{d_{sa} + d_{ac} - v_{sa} t_{sa} - v_{ac} t_{ac}}{2\sqrt{D_{Lsa} t_{sa} + D_{Lac} t_{ac}}} \right) \right. \\
&\quad \left. - \operatorname{erf}\left(\frac{d_{sa} + d_{ac} - v_{sa} t_{sa} - v_{ac} t_{ac} \pm v_{sa} t_g}{2\sqrt{D_{Lsa} t_{sa} + D_{Lac} t_{ac}}} \right) \right] \qquad (16)
\end{aligned}
$$

where $d_{sa} + d_{ac}$ is the distance from the shutter grid to the ion collector, and q is the coulombic charge associated with the singly or multiply charged ions. The total ion current arriving at the collector is obtained by multiplying Eq. (16) by A_c, the cross-sectional area of the ion collector (assumed equal to the cross-sectional area of the drift tube).

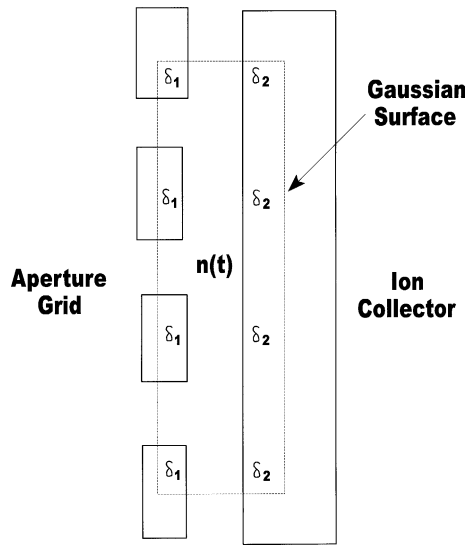

Fig. 4. An illustration showing a pillbox superimposed on the aperture grid/ion collector assembly to help calculate the surface charges (δ_1 and δ_2) induced on the aperture grid and collector, respectively.

3.2. Induced current flow

The induced current flow is calculated by applying Gauss's law [31] to Eq. (15). This is illustrated in Fig. 4 where a cross-section of the aperture grid/collector assembly with a superimposed "pillbox" is shown. Gauss's law states that the surface integral $\int \mathrm{d}\vec{S}$ of the electric field over the "pillbox" is equal to the charge q' contained within the "pillbox". That is

$$\varepsilon_0 \int \vec{E} \bullet \mathrm{d}\vec{S} = q' \qquad (17)$$

where ε_0 is the permittivity constant for free space. Induction effects are calculated by setting q' equal to 0, so that the total charge inside the "pillbox" is

$$q' = 0 = q \int n(r, z, t)\, \mathrm{d}V + \int (\delta_1 + \delta_2)\, \mathrm{d}A \qquad (18)$$

where δ_1 and δ_2 are the surface charges induced on the aperture grid and ion collector, respectively, and $\mathrm{d}V$ and $\mathrm{d}A$ are the differential volume and area of the "pillbox". Assuming field lines *will* escape the "pillbox", Eq. (18) can be rewritten as

$$\delta_1 + \delta_2 = -qw \int n(r, z, t)\, \mathrm{d}z \qquad (19)$$

where w is a weighting factor. The weighting factor (an number between 0 and 1) describes the number of field lines emitted by the ions that will terminate on either the aperture grid or ion collector electrodes of the IMS. Thus, w is equal to 1 if all the field lines terminate on the electrodes (i.e., no field lines escape from the ends of the aperture grid/ion collector assembly), and <1 if they do not. Due to the large aspect ratios typically associated with the aperture grid/collector assembly within an IMS, w is close to 1.

Because only the current flowing in the electrometer circuit is of interest, δ_2 is more important than δ_1. On the other hand, $\delta_1 \simeq \delta_2$ and Eq. (19) can be rewritten as

$$\delta_2 = -\frac{qw}{2}\int n(r,z,t)\,\mathrm{d}z \tag{20}$$

Since the first derivative of δ_2 is proportional to the induced current flow registered by the electrometer circuit, the current satisfies

$$J_{\text{induced}}A_c = \frac{\mathrm{d}\delta_2}{\mathrm{d}t} = -\frac{1}{2}qwA_c\frac{\mathrm{d}}{\mathrm{d}t}\int_{d_{sa}}^{d_{sa}+d_{ac}} n(r,z,t)\,\mathrm{d}z$$

$$= -\frac{1}{2}qwA_c v_{ac} n(r,z,t)\Big|_{d_{sa}}^{d_{sa}+d_{ac}} \tag{21}$$

The negative sign indicates that the initial direction of induced current flow is the same as the direct current flow as described in Section 2.2. When Eq. (15) is substituted into Eq. (21), the induced current flow satisfies

$$J_{\text{induced}}$$

$$= \pm\frac{wn_0T_iqv_{ac}}{4}\left[\operatorname{erf}\left(\frac{d_{sa}+d_{ac}-v_{sa}t_{sa}-v_{ac}t_{ac}}{2\sqrt{D_{Lsa}t_{sa}+D_{Lac}t_{ac}}}\right)\right.$$

$$-\operatorname{erf}\left(\frac{d_{sa}+d_{ac}-v_{sa}t_{sa}-v_{ac}t_{ac}\pm v_{sa}t_g}{2\sqrt{D_{Lsa}t_{sa}+D_{Lac}t_{ac}}}\right)$$

$$-\operatorname{erf}\left(\frac{d_{sa}-v_{sa}t_{sa}-v_{ac}t_{ac}}{2\sqrt{D_{Lac}t_{sa}+D_{Lac}t_{ac}}}\right)$$

$$\left.+\operatorname{erf}\left(\frac{d_{sa}-v_{sa}t_{sa}-v_{ac}t_{ac}\pm v_{sa}t_g}{2\sqrt{D_{Lsa}t_{sa}+D_{Lac}t_{ac}}}\right)\right] \tag{22}$$

Note the difference between two pairs of error functions whose arguments differ by only $d_{ac}/2\sqrt{D_{Lsa}t_{sa}+D_{Lac}t_{ac}}$. Already we can anticipate that d_{ac}, the separation between the ion collector and aperture grid, may contribute significantly to the resolving power of an IMS.

3.3. Total current flow

Since the total current registered by the electrometer circuit is the sum of both the direct and induced current flows, Eqs. (16) and (22) allow the total current to be written as

$$J_{\text{total}} = \mp\left(\frac{n_0T_iqv_{ac}}{2}-\frac{wn_0T_iqv_{ac}}{4}\right)$$

$$\times\left[\operatorname{erf}\left(\frac{d_{sa}+d_{ac}-v_{sa}t_{sa}-v_{ac}t_{ac}}{2\sqrt{D_{Lsa}t_{sa}+D_{Lac}t_{ac}}}\right)\right.$$

$$\left.-\operatorname{erf}\left(\frac{d_{sa}+d_{ac}-v_{sa}t_{sa}-v_{ac}t_{ac}\pm v_{sa}t_g}{2\sqrt{D_{Lsa}t_{sa}+D_{Lac}t_{ac}}}\right)\right]$$

$$\mp\left(\frac{wn_0T_iqv_{ac}}{4}\right)\left[\operatorname{erf}\left(\frac{d_{sa}-v_{sa}t_{sa}-v_{ac}t_{ac}}{2\sqrt{D_{Lsa}t_{sa}+D_{Lac}t_{ac}}}\right)\right.$$

$$\left.-\operatorname{erf}\left(\frac{d_{sa}-v_{sa}t_{sa}-v_{ac}t_{ac}\pm v_{sa}t_g}{2\sqrt{D_{Lsa}t_{sa}+D_{Lac}t_{ac}}}\right)\right] \tag{23}$$

Fig. 5 shows a plot of Eq. (23). The solid line is the observed ion mobility peak, while the dashed and dotted lines are the direct and induced current flows, respectively. It is clear that the induced current flow (dotted curve) distorts significantly the ion mobility peak (dashed curve), shortening the observed drift time and increasing the FWHH (solid curve).

3.4. Expectation values (drift time)

The expectation values for the drift times, $\langle t_{sa}\rangle$ and $\langle t_{ac}\rangle$, are calculated using

$$\langle t_{sa}\rangle = \left.\frac{\int_{-\infty}^{\infty} t_{sa}J_{\text{total}}\,\mathrm{d}t_{sa}}{\int_{-\infty}^{\infty} J_{\text{total}}\,\mathrm{d}t_{sa}}\right|_{t_{ac}=\text{constant}} \tag{24}$$

$$\langle t_{ac}\rangle = \left.\frac{\int_{-\infty}^{\infty} t_{ac}J_{\text{total}}\,\mathrm{d}t_{ac}}{\int_{-\infty}^{\infty} J_{\text{total}}\,\mathrm{d}t_{ac}}\right|_{t_{sa}=\text{constant}} \tag{25}$$

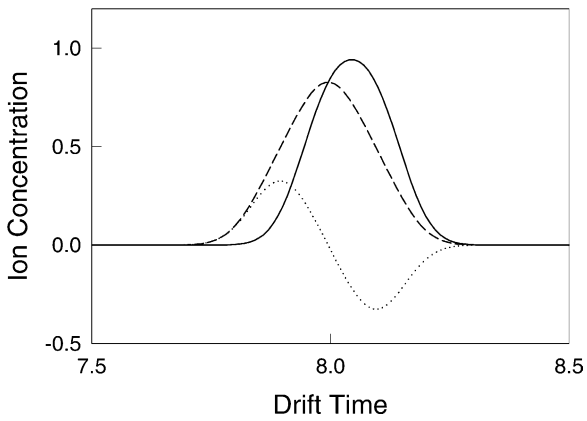

Fig. 5. A MathCAD plot showing the relative contributions of direct current flow (dashed line) and induced current flow (dotted line) to an ion mobility peak (solid line). The IMS parameters are those of Spangler and Collins [11] using a 200 μs gate width.

Applying the mathematical formalism described in Appendix B, the result is

$$\langle t_{sa}\rangle = \frac{d_{sa}}{v_{sa}} \pm \frac{t_g}{2}, \qquad \langle t_{ac}\rangle = \left(1 - \frac{w}{2}\right)\frac{d_{ac}}{v_{ac}} \tag{26}$$

It is important to note that $\langle t_{sa}\rangle$ calculated in this way is similar to Eq. (11). Also the effects of induced current flow is to subtract $wd_{ac}/2v_{ac}$ from t_{ac}, and hence from the total drift time $t_{sa} + t_{ac}$. This is intuitively correct since the maximum ion current registered by the electrometer should occur when the maximum ion concentration reaches the mid-plane between the aperture grid and ion collector.

3.5. Full-width-at-half-height

Depending on the IMS, the FWHH is calculated using one of two approaches. The first approach requires $v_{sa} \simeq v_{ac}$, while the second approach applies to any value for v_{sa} or v_{ac}, regardless of whether they are equal or not.

For $v_{sa} \simeq v_{ac}$, insertion of $\langle t_{sa}\rangle$ and $\langle t_{ac}\rangle$ into Eq. (23) yields

$$\begin{aligned} J_{\text{total,max}} = {} & \mp\left(\frac{n_0 T_i q v_{ac}}{2} - \frac{w n_0 T_i q v_{ac}}{4}\right) \\ & \times\left[\operatorname{erf}\left(\frac{wd_{ac} \mp v_{sa}t_g}{4\sqrt{D_{Lsa}t_{sa} + D_{Lac}t_{ac}}}\right)\right. \\ & \left. - \operatorname{erf}\left(\frac{wd_{ac} \pm v_{sa}t_g}{4\sqrt{D_{Lsa}t_{sa} + D_{Lac}t_{ac}}}\right)\right] \\ & \mp\left(\frac{w n_0 T_i q v_{ac}}{4}\right) \\ & \times\left[\operatorname{erf}\left(\frac{(w-2)d_{ac} \mp v_{sa}t_g}{4\sqrt{D_{Lsa}t_{sa} + D_{Lac}t_{ac}}}\right)\right. \\ & \left. - \operatorname{erf}\left(\frac{(w-2)d_{ac} \pm v_{sa}t_g}{4\sqrt{D_{Lsa}t_{sa} + D_{Lac}t_{ac}}}\right)\right] \end{aligned} \tag{27}$$

where $J_{\text{total,max}}$ is the maximum total ion current density arriving at the electrometer. Realizing that for a symmetric ion mobility peak, the half-height occurs at

$$t_{sa} + t_{ac} = \frac{d_{sa}}{v_{sa}} + \left(1 - \frac{w}{2}\right)\frac{d_{ac}}{v_{ac}} \pm \frac{t_g}{2} \pm \frac{\omega_h}{2} \tag{28}$$

the FWHH, ω_h, becomes

$$\begin{aligned} & \left(\frac{1}{4} - \frac{w}{8}\right)\left[\operatorname{erf}\left(\frac{wd_{ac} - v_{sa}t_g}{4\sqrt{D_{Lsa}t_{sa} + D_{Lac}t_{ac}}}\right)\right. \\ & \quad \left. -\operatorname{erf}\left(\frac{wd_{ac} + v_{sa}t_g}{4\sqrt{D_{Lsa}t_{sa} + D_{Lac}t_{ac}}}\right)\right] \\ & \quad + \left(\frac{w}{8}\right)\left[\operatorname{erf}\left(\frac{(w-2)d_{ac} - v_{sa}t_g}{4\sqrt{D_{Lsa}t_{sa} + D_{Lac}t_{ac}}}\right)\right. \\ & \left. -\operatorname{erf}\left(\frac{(w-2)d_{ac} + v_{sa}t_g}{4\sqrt{D_{Lsa}t_{sa} + D_{Lac}t_{ac}}}\right)\right] \\ & = \left(\frac{1}{2} - \frac{w}{4}\right)\left[\operatorname{erf}\left(\frac{wd_{ac} - v_{sa}t_g \pm v_{ac}\omega_h}{4\sqrt{D_{Lsa}t_{sa} + D_{Lac}t_{ac}}}\right)\right. \\ & \quad \left. -\operatorname{erf}\left(\frac{wd_{ac} + v_{sa}t_g \pm v_{ac}\omega_h}{4\sqrt{D_{Lsa}t_{sa} + D_{Lac}t_{ac}}}\right)\right] \\ & \quad + \left(\frac{w}{4}\right)\left[\operatorname{erf}\left(\frac{(w-2)d_{ac} - v_{sa}t_g \pm v_{ac}\omega_h}{4\sqrt{D_{Lsa}t_{sa} + D_{Lac}t_{ac}}}\right)\right. \\ & \left. -\operatorname{erf}\left(\frac{(w-2)d_{ac} + v_{sa}t_g \pm v_{ac}\omega_h}{4\sqrt{D_{Lsa}t_{sa} + D_{Lac}t_{ac}}}\right)\right] \end{aligned} \tag{29}$$

While Eq. (29) provides an exact relationship from which an exact value for the FWHH can be obtained, the components of ω_h are not easily distributed between the shutter/aperture and aperture/collector regions when $v_{sa} \neq v_{ac}$.

For $v_{sa} \neq v_{ac}$, a variance analysis must be performed and the second central moments calculated [32]

$$\sigma^2_{t_{sa}} = \left. \frac{\int_{-\infty}^{\infty} [t_{sa} - (d_{sa}/v_{sa}) \pm (t_g/2)]^2 \times J_{total}\, dt_{sa}}{\int_{-\infty}^{\infty} J_{total}\, dt_{sa}} \right|_{t_{ac}=\text{constant}} \quad (30)$$

$$\sigma^2_{t_{ac}} = \left. \frac{\int_{-\infty}^{\infty} [t_{ac} - (1-(w/2)) \times (d_{ac}/v_{ac})]^2 J_{total}\, dt_{ac}}{\int_{-\infty}^{\infty} J_{total}\, dt_{ac}} \right|_{t_{sa}=\text{constant}} \quad (31)$$

Again applying the mathematical formalism described in Appendix B, the computations yield

$$\sigma^2_{t_{sa}} = \frac{2(D_{Lsa} t_{sa} + D_{Lac} t_{ac})}{v^2_{sa}} + \frac{t_g^2}{12} + \left(\frac{w}{2} - \frac{w^2}{4}\right) \frac{d^2_{ac}}{v^2_{sa}} \quad (32)$$

$$\sigma^2_{t_{ac}} = \frac{2(D_{Lsa} t_{sa} + D_{Lac} t_{ac})}{v^2_{ac}} + \frac{v^2_{sa}}{v^2_{ac}} \frac{t_g^2}{12} + \left(\frac{w}{2} - \frac{w^2}{4}\right) \frac{d^2_{ac}}{v^2_{ac}} \quad (33)$$

Since t_{sa} and t_{ac} are independent variables, the total variance, $\sigma^2_{t_{sa}+t_{ac}}$, is given by

$$\sigma^2_{t_{sa}+t_{ac}} = \left(1 + \frac{v^2_{sa}}{v^2_{ac}}\right) \left[\frac{2(D_{Lsa} t_{sa} + D_{Lac} t_{ac})}{v^2_{sa}} + \frac{t_g^2}{12} + \left(\frac{w}{2} - \frac{w^2}{4}\right) \frac{d^2_{ac}}{v^2_{sa}} \right] \quad (34)$$

The FWHH is related to $\sigma^2_{t_{sa}+t_{ac}}$ through

$$\omega_h = A \sigma_{t_{sa}+t_{ac}} \quad (35)$$

where A is an adjustable parameter that allows Eq. (35) to agree with Eq. (29) when Eq. (35) is substituted into the error functions of Eq. (29). Unfortunately, the value associated with A cannot be known a priori, and depends on the operating parameters for the IMS cell. The only thing that can be said is that it must be greater than 2.354, the value it assumes for a Gaussian peak when $v_{ac} \gg v_{sa}$.

Before leaving this section, it should be noted that the definitions of Eqs. (30) and (31) differ from those of Urquijo et al. [28]. The present definition is more consistent with statistical variance that is related to the second central moment [32], an important point if the variances are going to be added as they are in Eq. (34).

4. Application

Three sets of data are available to test the predictive capabilities of the present theory. Spangler and Collins studied the dependence of the FWHH on the gate width using an early design of PCP, Inc.'s [33] line of ion mobility spectrometers [11]. Eiceman et al. studied the dependence of the FWHH on the drift potentials applied to the shutter and aperture grids [22]. Siems et al. studied the functional dependence of resolving power on the operating parameters of their IMS cell's [4].

4.1. Spangler and Collins

The significant operating parameters used by Spangler and Collins are shown in Table 1. A feature of their IMS cell was that the electric fields applied to the shutter/aperture and aperture/collector regions were approximately equal. This means that their FWHH data can be analyzed using Eq. (29). The result of the analysis is shown in Table 2 where the longitudinal

Table 1
Parametric data for Spangler and Collins' IMS cell [11]

Length of drift region	7.9 cm
Separation between aperture grid and ion collector	0.1 cm
Potential between shutter and aperture grids	1691 V
Potential between aperture grid and ion collector (see text)	21.4 V
Gate width (shutter grid)	Variable
Drift temperature	433.15 K
Reduced mobility of chloride ion studied	2.97–2.98 $cm^2\ V^{-1}\ s^{-1}$

Table 2
Comparison of peak-widths-at-half-height

Gate width, t_g (ms)	Measured peak width, ω_h (ms)	Calculated peak width, ω_h (ms)		Adjusted peak width, $v_{sa} = 0.87 v_{ac}$	A-value ($w = 1$)
		$w = 1$	$w = 0$		
0.05	0.20	0.2020	0.1285	0.2250	1.921
0.10	0.22	0.2065	0.1435	0.2290	2.000
0.20	0.27	0.2355	0.2077	0.2610	2.063
0.50	0.57	0.5000	0.5000	0.5555	2.494
1.00	1.09	1.0000	1.0000	1.1110	2.587

diffusion coefficient is calculated from ion mobility using the Einstein relationship [34]. For $w = 1$, there is good agreement between the experimental and theoretical results. The success is attributed to corrections made by the theory for induced ion current flow, as illustrated by the calculations for $w = 0$. A closer inspection of the data shows that the measured peak widths exceed calculated peak widths by about 10%. Calculations in the fifth column of Table 2 demonstrate that an ion velocity slightly greater in the shutter/aperture region than in the aperture/collector region can lead to this type of result. A very good way to compensate for peak broadening is to adjust the aperture/collector potential.

The A-values required to fit Spangler and Collins' data to Eqs. (34) and (35) appear in the last column of Table 2. As the gate width increases, the values increases to about $A = 2.6$. Assuming $v_{sa} = v_{ac}$, this value corresponds to a β of 1.13 (i.e., $2 \times (2.6)^2/12$), slightly less than similar values reported by Siems et al. [4].

4.2. Eiceman, Nazarov, Rodriguez and Stone

The significant operating parameters used by Eiceman et al. are recorded in Table 3. Because Eiceman et al. varied the electric fields in both the shutter/aperture and aperture/collector regions, Eq. (29) cannot be used to fit their data. Rather, Eqs. (34) and (35) must be used that require knowledge of d_{ac}. Although Eiceman et al. reported a value of 0.5 mm for the distance between their aperture grid and ion collector, the uncertainty associated with the stated

Table 3
Parametric data for Eiceman, Nazarov, Rodriguez and Stones' IMS cell [22]

Length of drift region	5.25 cm
Separation between aperture grid and ion collector	0.05 cm (nominal)
Potential between shutter and aperture grids	Variable
Potential between aperture grid and ion collector	Variable
Gate width (shutter grid)	208 μs
Drift temperature	523 K
Reduced mobility of positive reactant ion studied, K_0	2.49–2.73 $cm^2\ V^{-1}\ s^{-1}$

distance is large. Consequently, there is a need to determine this distance using another approach. This can be accomplished by fitting Eiceman et al.'s drift time data to Eq. (26). Unfortunately, Eiceman et al. are also uncertain about the distance between their shutter and aperture grids (d_{sa}). They give a value of 51 mm for d_{sa}, while at the same time giving a value of 5.25 cm for the total drift length ($d_{sa} + d_{ac}$) in Section E of their paper. Since the latter value was given when discussing the effects of electric field on the aperture/collector region, a value of 5.25 cm (5.25 cm − 0.5 mm) is assumed for d_{sa} in the present paper.

Figs. 6 and 7 show the results of fitting Eiceman et al.'s drift time data to $\langle t_{sa} \rangle + \langle t_{ac} \rangle$ in Eq. (26). The plots were generated by varying d_{ac}, and the mobility of the positive reactant ions adjusted to obtain a "visually pleasing" fit to both the shutter/aperture and aperture/collector data. As this was being done, it became apparent that the best value for d_{ac} was 0.288 mm. However, both sets of data

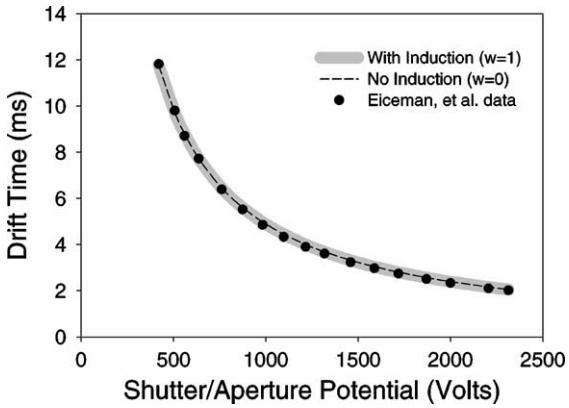

Fig. 6. Application of Eq. (26) to describe the drift time vs. shutter/aperture potential data of Eiceman et al. [22].

could not be fitted with the same mobility value for the ions. Rather the shutter/aperture data (Fig. 6) required a reduced mobility value of 2.49 $cm^2\,V^{-1}\,s^{-1}$, and the aperture/collector data required a reduced mobility value of 2.73 $cm^2\,V^{-1}\,s^{-1}$. By comparison, Eiceman et al. reported a reduced mobility range of 2.75–2.59 $cm^2\,V^{-1}\,s^{-1}$ for their aperture/collector data. Although the present values lie on either end of this range, a continuous decrease with reduced voltage is not observed.

To explore this further, the thermo-chemistry associated with the positive reactant ions was studied and applied to ion transport through the drift tube. The

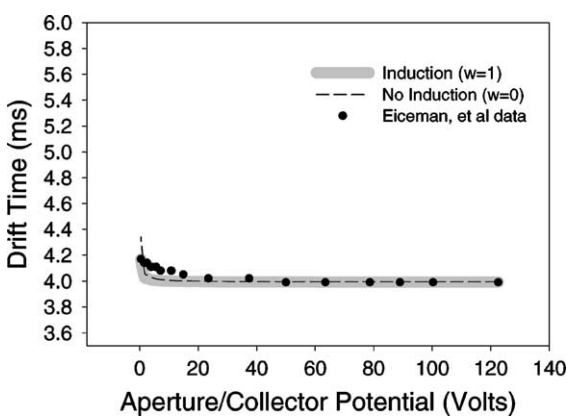

Fig. 7. Application of Eq. (26) to describe the drift time vs. aperture/collector potential data of Eiceman et al. [22].

theory is summarized in Appendix A. Since Eiceman et al. reported a moisture content or 0.1–0.2 ppm for their drift gas, it is possible to calculate their ion distribution and obtain a mobility for their rapidly exchanging hydrate ions. The results are shown in Table 4 for the two drift field conditions highlighted by Eiceman et al. Only two major proton hydrates, $(H_2O)H^+$ and $(H_2O)_2H^+$, are present (as Eiceman et al. acknowledge); but when Eq. (A.5) is further applied, the overall reduced mobility increases only 0.01 $cm^2\,V^{-1}\,s^{-1}$ ($2.60-2.59\,cm^2\,V^{-1}\,s^{-1}$) when the electric field (E_D) is increased from 80 to 440 $V\,cm^{-1}$. This negates the change in ion identity that Eiceman et al. assumed had to occur to explain the mobility variations observed in their data. The present theory suggests that the ion mobility is constant, and the apparent changes in ion mobility observed by Eiceman et al. are impossible. Perhaps Eiceman et al. were misled by the elementary theory they applied to the analysis of their data. Figs. 8 and 9 show the results of fitting Eqs. (34) and (35) to Eiceman et al.'s FWHH data. The fits are reasonable, considering the uncertainty in drift lengths noted above. Unlike Spangler and Collins, a value of 4.78 was needed for A to fit the shutter/aperture data (Fig. 8), and a value of 4.36 was needed for A to fit the aperture/collector data (Fig. 9). These large A-values can only be interpreted as additional factors contributing to peak broadening in Eiceman et al.'s experiments. This occurred despite the fact that Eiceman et al. used two parallel planes of juxtapositioned wires for their shutter grid that should have narrowed the peak width [25]. This is clearly evidenced by the Gaussian peak shape observed by Eiceman et al. when they applied a 0.208 μs wide pulse to their shutter grid, compared to the more nearly square peak observed by Spangler and Collins when using a 100 μs wide pulse. The source for the additional broadening is not clear. Some of it may be due to broadening produced by the convex bulge in the aperture grid that creates a variable distance between the aperture grid and collector (violating the parallelism assumption of the present theory), an ion collector diameter less than the diameter associated with the transmission area of the aperture grid (violating the equivalency of cross-sections

Table 4
Reduced mobilities for the hydrated hydronium ion with percent contributions for 0.15 ppm water in drift gas

Ion	Reduced mobility ($cm^2\,V^{-1}\,s^{-1}$)	Relative contribution ($E_D = 80\,V\,cm^{-1}$) (%)	Relative contribution ($E_D = 440\,V\,cm^{-1}$) (%)
H_3O^+	3.79	5.8	5.9
$(H_2O)H_3O^+$	2.52	94	94
$(H_2O)_2H_3O^+$	2.01	0.05	0.049
$(H_2O)_3H_3O^+$	1.72	10^{-7}	10^{-7}
$(H_2O)_4H_3O^+$	1.52	0	0
$(H_2O)_5H_3O^+$	1.38	0	0

assumption of the present theory), or the non-linear fringe field that exists in their stacked ring drift tube (violating the uniform field assumption of the present theory). The aperture grid bulge may also explain why a higher ion mobility was required to fit the drift times associated with the aperture/collector potential data.

4.3. Siems, Wu, Tarver, Hill, Larsen and McMinn

Siems et al. observed that the diffusion broadening of their IMS peaks was greater than expected for ideal conditions. They found that they had to multiply their diffusion terms by a factor α that was greater than the ideal value of $0.957 \times 10^{-3}\,V\,K^{-1}$. Because of the elevated values for α, they felt that other diffusion-like processes were occurring in their IMS cell. Using an *A*-value of 2.6 that was found necessary to fit Spangler and Collins' data to Eqs. (34) and (35), the present theory suggests that α should be greater than approximately 1.21 ($(2.6)^2/8 \times \ln 2$). The amount it exceeds 1.21 is dependent on the value of $1 + (v_{sa}^2/v_{ac}^2)$, or the way the IMS cell is biased. Also note that the induction term, $[(w/2) - (w^2/4)](d_{ac}^2/v_{sa}^2)$, has an inverse velocity dependence that makes it look like a diffusion term. Hence, Siems et al. were correct when they postulated that other diffusion-like processes were occurring in their IMS cell. By comparison, Eiceman et al.'s data are characterized by an α of 4.08 [$1.21 \times ((4.78)^2/(2.6)^2)$] that is within the 1.26–6.5 range observed by Siems et al.

Siems et al. further noted that the square of their peak width was a linear function of their diffusion term (Tt_d^2/V) with an intercept dependent on the gate width t_g. Eqs. (34) and (35) suggest that this intercept varies as t_g^2, and is amplified by $(1/12)[1 + (v_{sa}^2/v_{ac}^2)]$. This means that the slope of Siems et al.'s data should

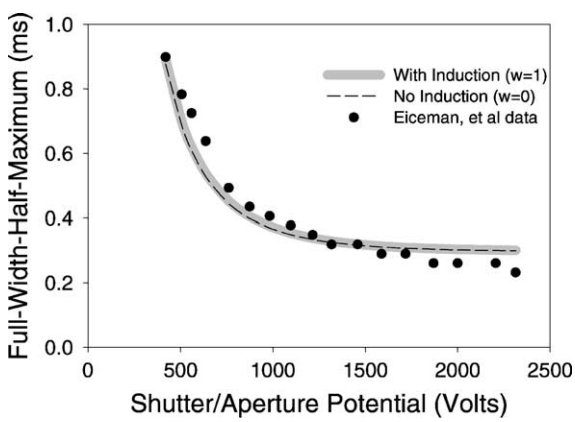

Fig. 8. Application of Eq. (35) to describe the FWHH vs. shutter/aperture potential data of Eiceman et al. [22].

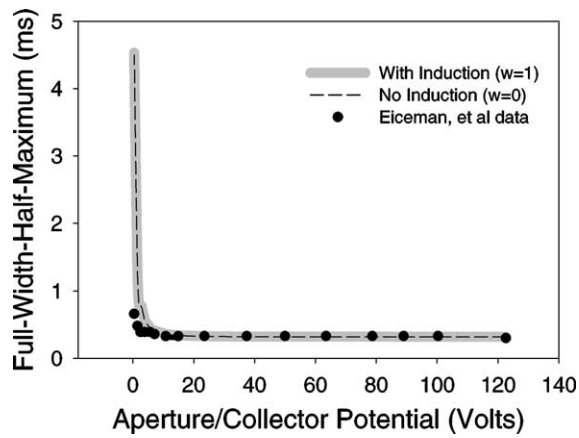

Fig. 9. Application of Eq. (35) to describe the FWHH vs. aperture/collector potential data of Eiceman et al. [22].

depend on the drift field, particularly if the shutter/aperture and aperture/collector potentials are varied independently. The field dependence is not observed, however, if the two fields are varied proportionately.

Finally, Siems et al. observed that the square of their peak width was a linear function of t_g^2 and the intercept was inversely proportional to the applied drift field. Again, Eqs. (34) and (35) indicate that these intercepts should vary as the inverse of the cube of the applied drift field (diffusion term) and the square of the drift field (induction term). Since the strength of the diffusion term is much greater than the induction term, the intercept is most likely controlled by the diffusion term.

The present theory does not explain Siems et al.'s need for a small correction term, γ, to fit their FWHH data. Perhaps this reflects the inaccuracies of the incomplete theory used by Siems et al. to fit their data.

4.4. Other comments

Most of the attention of this paper has been given to the separation between the aperture grid and ion collector, and the effect that the separation has on the FWHH of the ion mobility peak. This is not to ignore the fact that Eqs. (1) and (5) clearly indicate that the elapsed drift time or the length of the drift tube also influences the resolving power of the IMS. In fact, the inefficiencies associated with the design of the aperture/collector region can be compensated by a longer drift tube, and vice versa. Because competing philosophies exist regarding the best approach to electrically bias an IMS cell (e.g., aperture/collector and shutter/aperture potentials equal, vs. aperture/collector potential greater than shutter/aperture potential), clear statements on designing and biasing an IMS cell cannot be made. However, lengthening the drift tube, and narrowing the gap between the aperture grid and ion collector should improve the resolving power of an IMS. Additional gains are also possible from the way the IMS cell is biased.

The discussion has also not taken into consideration the time constant, τ, that may be associated with the response of the electrometer. For the work sighted in this paper, this time constant appears to be on the order of 35–100 μs (per the specifications of the Keithley current amplifier). Such a time constant introduces an additional term $2D_L(t_{sa}+t_{ac})/v_{ac}\tau$ into the error functions that could potentially contribute to the FWHH; but when divided by v_{sa}, the term is approximately equal to 2 μs, much less than the observed FWHH's. It is therefore believed that the time constants make a negligible contribution to the results. However, this conclusion is not generally correct, and the time constants for the electrometer are always an important issue when analyzing IMS resolution data.

5. Conclusions

An expanded theory for the resolving power of a linear IMS cell has been developed. By definition, the resolving power is directly proportional to the total drift time for the ion through the drift tube divided by the FWHH of the observed ion mobility peak. Two approaches can be taken to theoretically analyze resolving power. If the electric fields are equal in the shutter/aperture and aperture/collector regions of the IMS cell, the FWHH can be calculated from a difference in error functions. If the electric fields are not equal, the FWHHs can be calculated to within a multiplicative factor using the second central moment of the IMS response. The drift times are calculated from the first moment of the IMS response in each case. The effectiveness of these approaches is illustrated by the data in Figs. 6–9.

The additional peak broadening often observed in an IMS cell has a variety of possible sources. One depends on the construction of the cell and the parallelism (or lack thereof) that might exist between the aperture grid and ion collector. Another is the uniformity of the electric field in the IMS cell. Still another is the distribution of the electric field used to bias the cell. If the electric field in the aperture/collector region is less than in the shutter/aperture region, apparent peak broadening can occur. Induction effects in the aperture/collector region not only shorten drift times, but

also create diffusion-like broadening of the ion mobility peak. Shortening the distance between the aperture grid and ion collector, or using a higher electric field in that region minimizes induction effects. Drift time calibration requires full use of Eq. (26).

Acknowledgements

The author wishes to acknowledge discussions and data exchanges with Dr. Erkinjon G. Nazarov of New Mexico State University. Dr. Nazarov kindly provided the original test data used in [22]. Dr. Nazarov also answered a number of questions concerning the biasing of the IMS cell that was incompletely described in [22]. His contributions greatly improved the integrity of this work.

Appendix A

Often the terminal ions created in an ion mobility spectrometer operated under atmospheric pressure conditions are solvated with adduct molecules. The most common adducts are one or more water molecules derived from the trace water contained in the carrier and drift gases. The extent of solvation is controlled by the equilibrium

$$(\mathrm{S})_{i-1}\mathrm{I}^{\pm} + \mathrm{S} + \mathrm{M} \rightleftharpoons (\mathrm{S})_i\mathrm{I}^{\pm} + \mathrm{M} \tag{A.1}$$

where $\mathrm{I}^{\pm}$ is the ion, S the solvent molecule, M a third collision partner involved in thermalizing the activated complex, and "*i*" is the number of solute molecules attached to the ion. The reaction rate constants are often fast, allowing the solvated ions, regardless of *i*, to travel down the drift tube as a rapidly exchanging ion mixture in local equilibrium. While there are also important cases where the forward and reverse rate constants are not fast, these cases are not considered in this presentation.

As a result of the rapidly exchanging equilibrium, the ionic charge spends a portion of its drift time as an $(\mathrm{S})_i\mathrm{I}^{\pm}$ ion, another portion of its drift time as another *i*th ion, etc. The fractional amount of time spent for each degree of solvation has been shown to be proportional to the equilibrium mole fraction x_i, such that $\sum_i x_i = 1$ [35]. As the equilibrium shifts, the velocity or observed drift time for the ion mixture changes with the solvent (or water) concentration.

If the drift length for the drift tube is l_d, the drift velocity v_d is given by

$$v_\mathrm{d} = \frac{l_\mathrm{d}}{t_\mathrm{obs}} \tag{A.2}$$

where t_obs is the observed drift time. Rearranging, Eq. (A.2) becomes

$$l_\mathrm{d} = v_\mathrm{d} t_\mathrm{obs} = \sum_n x_i v_{\mathrm{d}i} t_i \tag{A.3}$$

where the summation is over all significant solvated ions. Depending on the objectives of the authors, Eq. (A.3) can be analyzed in different ways. If the objective is to study the kinetics of the ion–molecule reactions, the component $v_{\mathrm{d}i}$'s of Eq. (A.3) are assumed equal to v_d, and the mole fraction ratios x_i associated with the t_i's. The t_i's then become the drift times for the component ions of the migrating ion cloud as if the exchange reactions were not occurring. This approach was developed by Giles and Grimsrud and further applied by Sahlstrom et al. and Lawrence et al. [36–38]. If the objective is to study the transport properties of the ions, the component t_i's in Eq. (A.3) are assumed equal to t_obs, and the mole fraction ratios x_i's associated with the $v_{\mathrm{d}i}$'s. The $v_{\mathrm{d}i}$'s then become the drift velocities for the component ions of the migrating ion cloud as if the exchange reactions were not occurring. This approach was first developed by Woo and Whealton [39] and Iinuma [40], and further applied by Spangler [41]. Since ion transport mechanisms is the subject of the present paper, the latter approach is of interest.

Eq. (A.3) can be further simplified to

$$v_\mathrm{d} = KE = \sum_n x_i K_i E \tag{A.4}$$

where $K_i E$ is equal to $v_{\mathrm{d}i}$ and the K_i's are the traditional mobilities for the component ions. When the electric field E on both sides of Eq. (A.4) is canceled

$$K = \sum_n x_i K_i \tag{A.5}$$

where K is the mobility of the exchanging ion mixture drifting through the drift tube.

The equilibrium constants associated with the freely exchanging ions traveling in local equilibrium are

$$K_{n-1,n} = \frac{[(\mathrm{S})^n\mathrm{I}^{\pm}]}{[(\mathrm{S})^{n-1}\mathrm{I}^{\pm}]}\frac{P_0}{P_\mathrm{S}} = \exp\left(-\frac{\Delta G^\circ_{n-1,n}}{RT}\right) \tag{A.6}$$

where S is the solvent molecule, P_S its partial pressure, P_0 the standard pressure (i.e., 1.0 atm), $\Delta G^\circ_{n-1,n}$ the free energy released when adding one solvent molecule to the ion, and T is the drift temperature. Because the ion concentrations of Eq. (A.6) can be expressed in terms of the total concentration n_T using

$$\begin{aligned}
&[\mathrm{I}^{\pm}] = x_{\mathrm{I}^{\pm}} n_T \\
&[(\mathrm{S})\mathrm{I}^{\pm}] = x_{(\mathrm{S})\mathrm{I}^{\pm}} n_T \\
&\vdots \\
&[(\mathrm{S})^n\mathrm{I}^{\pm}] = x_{(\mathrm{S})^n\mathrm{I}^{\pm}} n_T
\end{aligned} \tag{A.7}$$

The mole fractional ratios become

$$\begin{aligned}
x_{\mathrm{I}^{\pm}} &= \frac{[\mathrm{I}^{\pm}]}{[\mathrm{I}^{\pm}] + [(\mathrm{S})\mathrm{I}^{\pm}] + \cdots + [(\mathrm{S})^m\mathrm{I}^{\pm}]} \\
x_{(\mathrm{S})\mathrm{I}^{\pm}} &= \frac{[(\mathrm{S})\mathrm{I}^{\pm}]}{[\mathrm{I}^{\pm}] + [(\mathrm{S})\mathrm{I}^{\pm}] + \cdots + [(\mathrm{S})^m\mathrm{I}^{\pm}]} \\
&\vdots \\
x_{(\mathrm{S})^m\mathrm{I}^{\pm}} &= \frac{[(\mathrm{S})^m\mathrm{I}^{\pm}]}{[\mathrm{I}^{\pm}] + [(\mathrm{S})\mathrm{I}^{\pm}] + \cdots + [(\mathrm{S})^m\mathrm{I}^{\pm}]}
\end{aligned} \tag{A.8}$$

where the sum of x_i's over all the ions is equal to 1. When Eq. (A.6) is introduced into Eq. (A.8) [41],

$$\begin{aligned}
x_i &= \frac{(P_\mathrm{S}/P_0)^i K_{0,1}K_{1,2}\cdots K_{i-1,i}[\mathrm{I}^{\pm}]}{[\mathrm{I}^{\pm}] + (P_\mathrm{S}/P_0)K_{0,1}[\mathrm{I}^{\pm}] \\
&\quad + (P_\mathrm{S}/P_0)^2 K_{0,1}K_{1,2}[\mathrm{I}^{\pm}] + \cdots \\
&\quad + (P_\mathrm{S}/P_0)^m K_{0,1}K_{1,2}\cdots K_{m-1,m}[\mathrm{I}^{\pm}] \\
&= \frac{(P_\mathrm{S}/P_0)^i \prod_{n=0}^{i} K_{n-1,n}}{\sum_m (P_\mathrm{S}/P_0)^m \prod_{n=0}^{m} K_{n-1,n}} \\
&= \frac{(P_\mathrm{S}/P_0)^i \prod_{n=0}^{i} \exp(-\Delta G^\circ_{n-1,n}/RT)}{\sum_m (P_\mathrm{S}/P_0)^m \prod_{n=0}^{m} \exp(-\Delta G^\circ_{n-1,n}/RT)}
\end{aligned} \tag{A.9}$$

where $m \geq i$, $K_{-1,0} \equiv 1$. Since $\Delta G^\circ_{n-1,n}$ is given by $\Delta H^\circ_{n-1,n} - T\,\Delta S^\circ_{n-1,n}$, it can be calculated from the enthalpy $\Delta H^\circ_{n-1,n}$ and entropy $\Delta S^\circ_{n-1,n}$ changes published by Kebarle [42].

Eqs. (A.4) and (A.9) provide an accurate description for the drift velocity of an exchanging ion mixture provided the ratio of the electric field to the number density of the drift gas (E/N) is small. If E/N gets large, the distribution function associated with the ions becomes skewed, showing evidence of non-equilibrium. When this occurs, it is necessary to define an effective drift temperature, $T_{\mathrm{eff,i}}$, that is used in place of the thermodynamic temperature, T, to adjust for the non-linear effects. This effective temperature, $T_{\mathrm{eff,i}}$, is given by [43]

$$T_{\mathrm{eff,i}} = T + \frac{1}{3}\frac{M v_{\mathrm{d}i}^2}{k} \tag{A.10}$$

where M is the mass of the colliding neutral gas molecule and k is the Boltzmann constant. The effective temperature must not only be applied to the equilibria described by Eqs. (A.6)–(A.9), but also to the ion mobilities contained in Eqs. (A.4) and (A.5).

To within an error of about 20%, the Chapman–Enskog result can be used to write down an expression for the ion mobilities [43]

$$\begin{aligned}
K_i &= \frac{3q}{16N}\left(\frac{2\pi}{\mu_\mathrm{i} k T_{\mathrm{eff,i}}}\right)^{1/2} \frac{1}{\Omega_\mathrm{i}^{(1,1)}(T_{\mathrm{eff,i}})} \\
&= \frac{3q}{16P}\left(\frac{2\pi k T_{\mathrm{eff,i}}}{\mu_\mathrm{i}}\right)^{1/2} \frac{1}{\Omega_\mathrm{i}^{(1,1)}(T_{\mathrm{eff,i}})}
\end{aligned} \tag{A.11}$$

where q is the charge on the ion, N and P the number density and pressure for the drift gas, μ_i the reduced mass for the ion, $\Omega_\mathrm{i}^{(1,1)}$ the collision integral describing the ion–molecule interactions and k is the Boltzmann gas constant. The second expression follows from application of the ideal gas law. Substituting Eq. (A.10) into Eq. (A.11) and solving for K_i yields

$$K_i = \frac{3q(2\pi kT)^{1/2}}{\sqrt{256\mu_\mathrm{i} P^2 (\Omega_\mathrm{i}^{(1,1)}(T_{\mathrm{eff,i}}))^2 - 6\pi q^2 M E^2}} \tag{A.12}$$

There is considerable confusion over the value that should be used for the collision integral, $\Omega_i^{(1,1)}(T_{\mathrm{eff,i}})$, in the open scientific literature [44–50]. When studying the mobility of protonated amines in helium, air, CO_2 and SF_6, Karpas et al. found that neither the rigid-sphere or polarization limit models reproduced their experimental data [51]. To fit their data, they replaced the critical impact parameter, b_0 [52]

$$b_0 = \frac{4q^2\alpha_p}{\mu_r v_{r_0}} \tag{A.13}$$

with an adjustable parameter $r_m = (r_0 + zm_{\mathrm{eff}})[1 + (m_{\mathrm{eff}}/M)^{1/3}]$ that increased with both the mass of the ion and the mass of the drift gas molecules. In Eq. (A.13), q is the charge on the ion, α_p the polarizability of the colliding neutral gas molecule, μ_r the reduced mass ion–molecule pair, and v_{r_0} is the initial velocity of the ion relative to the neutral molecule; and for r_m, r_0 is an adjustable constant, m_{eff} is an effective mass of the ion that takes into account clustering, and M is the mass of colliding gas molecules. When studying the trialkyl-amines, Spangler favored the rigid sphere model when fitting his data [53]. Additional studies have confirmed the usefulness of this approach, as well as the assumption that the density of "ionic matter" is constant [54]. When these assumptions are applied, the collision integral can be written as

$$\Omega_{(S)_i I^{\pm}} = \pi \left[\left(\frac{3V_{(S)_i I^{\pm}}}{4\pi N_A} \right)^{1/3} + \left(\frac{3V_M}{4\pi N_A} \right)^{1/3} \right]^2 \tag{A.14}$$

where $V_{(S)_i I^{\pm}}$ and V_M are the molar volumes for the ions and neutral collision partners, respectively, and N_A is Avogadro's number.

Eq. (A.14) transfers the task of estimating the collision cross-section to finding appropriate values for the molar volumes. Initial attempts at using van der Waal's volumes [55], crystallographic volumes, and molar volumes deduced from molecular modeling [56] (as implemented in "Molecular Modeling Pro" from ChemSW, Inc., Fairfield, CA) have been unsuccessful. Rather greater success has been achieved using data deduced from densities near the boiling point. Schroeder has shown that such data can be described using incremental volumes for the atomic constituents of the molecular species under investigation [57,58]. For example, hydrogen and oxygen both have incremental molar volumes 7 $\mathrm{cm^3\,g\text{-}mol^{-1}}$, so that the molar volume for water is 21.5 $\mathrm{cm^3\,g\text{-}mol^{-1}}$. Similarly, nitrogen atoms have incremental molar volumes 7 $\mathrm{cm^3\,g\text{-}mol^{-1}}$, so that the molar volume for a nitrogen molecule is 28 $\mathrm{cm^3\,g\text{-}mol^{-1}}$ (the triple bond in a nitrogen molecule is equivalent to 14 $\mathrm{cm^3\,g\text{-}mol^{-1}}$). While the experience with this approach is limited (particularly the temperature dependence of such an approach), it was used to calculate the reduced mobilities and ion distributions reported in Table 4 of the main paper.

Table 4 of the main paper was generated by first estimating the molar volumes for each ion participating in the exchanging ion mixture using the method of Schroeder, substituting the molar volumes into Eq. (A.14), inserting the collision cross-sections into Eq. (A.12), and then evaluating Eq. (A.9) using the mobilities obtained from Eq. (A.12).

Appendix B

This appendix describes an approach to solving equations of the type

$$\int_{-\infty}^{\infty} (t-\tau)^m \left[\mathrm{erf}\left(\frac{d - vt}{2\sqrt{Dt}} \right) - \mathrm{erf}\left(\frac{d - vt \pm vt_g}{2\sqrt{Dt}} \right) \right] \mathrm{d}t \tag{B.1}$$

where d is a location within the drift tube, t the drift time, t_g the gate width applied to the shutter grid, D and v the diffusion coefficient and drift velocity associated with the motion of the ion, and τ is a constant (0 when calculating expectation values, and a drift time when calculating variance). The exponent m assumes integer values between 0 and 2.

As illustrated by Eqs. (10) and (11) in the main text, Eq. (B.1) can be solved with reasonable accuracy by treating $\sqrt{Dt}$ as a constant. That is, the time variation of $\sqrt{Dt}$ can be ignored. Using this approach, the first

step to a solution is to change variables. This is accomplished by defining

$$z' \equiv \frac{d - vt}{2\sqrt{Dt}}, \qquad dz' = -\frac{v}{2\sqrt{Dt}}dt,$$
$$t = \frac{d - 2z'\sqrt{Dt}}{v} \tag{B.2}$$

and substituting Eq. (B.2) into Eq. (B.1). The result is

$$-\frac{2\sqrt{Dt}}{v}\int_{-\infty}^{\infty}\left(\frac{d - v\tau}{v} - \frac{2z'\sqrt{Dt}}{v}\right)^m \times\left[\operatorname{erf}(z') - \operatorname{erf}\left(z' \pm \frac{vt_g}{2\sqrt{Dt}}\right)\right]dz' \tag{B.3}$$

Eq. (B.3) contains two terms: a polynomial term, and a difference in error functions term.

The error function term is expanded with the aid of Taylor's theorem [59]

$$y = y_0 + (x - x_0)y_0' + \frac{(x - x_0)^2}{2!}y_0'' + \cdots + \frac{(x - x_0)^n}{n!}y_0^{(n)} \tag{B.4}$$

where y_0 is the function y evaluated at $x = x_0$, and $y_0^{(n)}$ is the nth derivative of y evaluated at $x = x_0$. When y is equal to $\operatorname{erf}(x_0 \pm \delta)$ and δ is small, Eq. (B.4) is equivalent to

$$\operatorname{erf}(x_0 \pm \delta) = \operatorname{erf}(x_0) + \sum_{n=0}^{\infty}\frac{(\pm\delta)^{n+1}}{(n+1)!}\frac{d^{n+1}}{dx^{n+1}}\operatorname{erf}(x)\bigg|_{x=x_0} \tag{B.5}$$

But [60]

$$\frac{d^{n+1}}{dx^{n+1}}\operatorname{erf}(x) = (-1)^n\frac{2}{\sqrt{\pi}}H_n(x)\,\mathrm{e}^{-x^2} \tag{B.6}$$

where $H_n(x)$ are the Hermite polynomials. Consequently, Eq. (B.5) becomes

$$\operatorname{erf}(x_0) - \operatorname{erf}(x_0 \pm \delta) = \frac{2}{\sqrt{\pi}}\sum_{n=0}^{\infty}\frac{(\mp\delta)^{n+1}}{(n+1)!}H_n(x_0)\,\mathrm{e}^{-x_0^2} \tag{B.7}$$

or when $x_0 = z'$ and $\delta = vt_g/2\sqrt{Dt}$, it becomes

$$\operatorname{erf}(z') - \operatorname{erf}\left(z' \pm \frac{vt_g}{2\sqrt{Dt}}\right) = \frac{2}{\sqrt{\pi}}\sum_{n=0}^{\infty}\frac{1}{(n+1)!}\left(\mp\frac{vt_g}{2\sqrt{Dt}}\right)^{n+1}H_n(z')\,\mathrm{e}^{-(z')^2} \tag{B.8}$$

When Eq. (B.8) is substituted into Eq. (B.3), the result is

$$-\frac{4}{v}\sqrt{\frac{Dt}{\pi}}\sum_{n=0}^{\infty}\frac{1}{(n+1)!}\left(\frac{\mp vt_g}{2\sqrt{Dt}}\right)^{n+1} \times\int_{-\infty}^{\infty}H_n(z')\,\mathrm{e}^{-(z')^2}\,\mathrm{d}z', \quad \text{for } m = 0 \tag{B.9}$$

$$-\frac{4d}{v^2}\sqrt{\frac{Dt}{\pi}}\sum_{n=0}^{\infty}\frac{1}{(n+1)!}\left(\frac{\mp vt_g}{2\sqrt{Dt}}\right)^{n+1} \times\int_{-\infty}^{\infty}H_n(z')\,\mathrm{e}^{-(z')^2}\,\mathrm{d}z' + \frac{8Dt}{v^2\sqrt{\pi}} \times\sum_{n=0}^{\infty}\frac{1}{(n+1)!}\left(\frac{\mp vt_g}{2\sqrt{Dt}}\right)^{n+1} \times\int_{-\infty}^{\infty}z'H_n(z')\,\mathrm{e}^{-(z')^2}\,\mathrm{d}z', \quad \text{for } m = 1 \text{ and } \tau = 0 \tag{B.10}$$

and

$$-\frac{4}{v}\sqrt{\frac{Dt}{\pi}}\left(\frac{d - v\tau}{v}\right)^2\sum_{n=0}^{\infty}\frac{1}{(n+1)!}\left(\frac{\mp vt_g}{2\sqrt{Dt}}\right)^{n+1} \times\int_{-\infty}^{\infty}H_n(z')\,\mathrm{e}^{-(z')^2}\,\mathrm{d}z' + \frac{16}{v^2\sqrt{\pi}}\left(\frac{d - vt}{v}\right) \times\sum_{n=0}^{\infty}\frac{1}{(n+1)!}\left(\frac{\mp vt_g}{2\sqrt{Dt}}\right)^{n+1} \times\int_{-\infty}^{\infty}z'H_n(z')\,\mathrm{e}^{-(z')^2}\,\mathrm{d}z' - \frac{16(Dt)^{3/2}}{v^3\sqrt{\pi}} \times\sum_{n=0}^{\infty}\frac{1}{(n+1)!}\left(\frac{\mp vt_g}{2\sqrt{Dt}}\right)^{n+1} \times\int_{-\infty}^{\infty}(z')^2H_n(z')\,\mathrm{e}^{-(z')^2}\,\mathrm{d}z', \quad \text{for } m = 2 \tag{B.11}$$

Contained within Eqs. (B.9)–(B.11) are integrals of the type

$$\int_{-\infty}^{\infty} (z')^p H_n(z')\, \mathrm{e}^{-(z')^2}\, \mathrm{d}z' \tag{B.12}$$

that must be evaluated.

Because the Hermite polynomials satisfy [61],

$$H_n(-z') = (-1)^n H_n(z') \tag{B.13}$$

Eq. (B.12) provides a non-zero solution only when $n + m$ is even. Furthermore, the orthogonality of the Hermite polynomials dictates that [62],

$$\int_{-\infty}^{\infty} H_n(z') H_m(z')\, \mathrm{e}^{-(z')^2}\, \mathrm{d}z' = \begin{cases} 0, & \text{for } m \neq n \\ 2^n \cdot n! \sqrt{\pi}, & \text{for } m = n \end{cases} \tag{B.14}$$

Applying Eq. (B.14) to Eq. (B.12) yields

$$\int_{-\infty}^{\infty} H_n(z')\, \mathrm{e}^{-(z')^2}\, \mathrm{d}z' = \int_{-\infty}^{\infty} H_0(z') H_n(z')\, \mathrm{e}^{-(z')^2}\, \mathrm{d}z' = \sqrt{\pi}, \quad \text{for } p = 0 \tag{B.15}$$

$$\int_{-\infty}^{\infty} z' H_n(z')\, \mathrm{e}^{-(z')^2}\, \mathrm{d}z' = \frac{1}{2} \int_{-\infty}^{\infty} H_1(z') H_n(z')\, \mathrm{e}^{-(z')^2}\, \mathrm{d}z' = \sqrt{\pi}, \quad \text{for } p = 1 \tag{B.16}$$

and

$$\int_{-\infty}^{\infty} (z')^2 H_n(z')\, \mathrm{e}^{-(z')^2}\, \mathrm{d}z' = \frac{1}{4} \int_{-\infty}^{\infty} [2H_0(z') + H_2(z')] H_n(z')\, \mathrm{e}^{-(z')^2}\, \mathrm{d}z' = \begin{cases} \dfrac{\sqrt{\pi}}{2}, & \text{for } n = 0 \\ 2\sqrt{\pi}, & \text{for } n = 2 \end{cases} \quad (\text{for } p = 2) \tag{B.17}$$

All other values of the integral are 0, regardless of the value of p.

When Eqs. (B.9)–(B.11) are combined with Eqs. (B.15)–(B.17), the results are summarized in Table B.1.

Table B.1
Values for Eq. (B.1)

Parameters	Eq. (B.1)
$m = 0$	$\pm 2t_g$
$m = 1;\ \tau = 0$	$\pm \dfrac{2dt_g}{v} + t_g^2$
$m = 2$	$\pm 2t_g \left(\dfrac{d - v\tau}{v}\right)^2 + 2t_g^2 \left(\dfrac{d - v\tau}{v}\right) \pm \dfrac{4Dt}{v^2} t_g \pm \dfrac{2}{3} t_g^3$

These results are used to evaluate the various integrals in the main text.

References

[1] H.H. Hill Jr., W.F. Siems, R.H. St. Louis, D.G. McMinn, Anal. Chem. 62 (1990) 1201A, and references therein.
[2] R.L. Grob, Modern Practice of Gas Chromatography, 3rd Edition, Wiley, New York, 1995, p. 42.
[3] S. Rokushika, H. Hatano, M.A. Baim, H.H. Hill Jr., Anal. Chem. 57 (1985) 1902.
[4] W.F. Siems, C. Wu, E.E. Tarver, H.H. Hill Jr., P.R. Larsen, D.G. McMinn, Anal. Chem. 66 (1994) 4195.
[5] J.P. Carrico, D.W. Sickenberger, G.E. Spangler, K.N. Vora, J. Phys. E: Sci. Instrum. 16 (1983) 1058.
[6] G.E. Spangler, K.N. Vora, J.P. Carrico, J. Phys. E: Sci. Instrum. 19 (1986) 191.
[7] L.M. Matz, H.H. Hill Jr., Anal. Chem. 74 (2002) 420.
[8] J.W. Dolan, LC/GC 20 (5) (2002) 430.
[9] J.H. Knox, L. McLaren, Anal. Chem. 35 (1963) 449.
[10] G. Gasper, R. Annino, C. Vidal-Madjar, G. Guiochon, Anal. Chem. 50 (1978) 1512.
[11] G.E. Spangler, C.I. Collins, Anal. Chem. 47 (1975) 403.
[12] P. Watts, A. Wilders, Int. J. Mass Spectrom. Ion Process. 112 (1992) 179.
[13] H.E. Revercomb, E.A. Mason, Anal. Chem. 47 (1975) 970.
[14] J.T. Moseley, I.R. Gatland, D.W. Martin, E.W. McDaniel, Phys. Rev. 178 (1969) 234.
[15] J. Xu, W.B. Whitten, J.M. Ramsey, Anal. Chem. 72 (2000) 5787.
[16] G.A. Eiceman, V.J. Vandiver, T. Chen, G. Rico-Martinez, Anal. Instrum. 18 (3/4) (1989) 227.
[17] J.T. Moseley, D.W. Martin, E.W. McDaniel, R.M. Snuggs, T.M. Miller, Technical Report, Georgia Institute of Technology, Atlanta, GA, 1968 (unpublished).
[18] J.H. Schummers, G.M. Thomson, D.R. James, I.R. Gatland, E.W. McDaniel, Phys. Rev. 66 (1973) 683.
[19] E.A. Mason, E.W. McDaniel, Transport Properties of Ions in Gases, Wiley, New York, 1988 (Chapter 6.2).
[20] M.J. Cohen, Private Communication, 1975.
[21] G.E. Spangler, Anal. Chem. 64 (1992) 1312.
[22] G.A. Eiceman, E.G. Nazarov, J.E. Rodriguez, J.A. Stone, Rev. Sci. Instrum. 72 (2001) 3610.

[23] D.L. Albritton, D.W. Martin, E.W. McDaniel, T.M. Miller, J.T. Moseley, Measurement of the Low-Energy Transport Parameters of Mass-Identified Ions in Gases; Mobilities of H_3^+ and H_1^+ Ions in Hydrogen, Technical Report, Georgia Institute of Technology, Atlanta, GA, 10 May 1967.
[24] C. Wu, W.E. Steiner, P.S. Tornatore, L.M. Matz, W.F. Siems, D.A. Atkinson, H.H. Hill Jr., Talanta 57 (2002) 123.
[25] G.E. Spangler, Anal. Chem. 65 (1993) 3010.
[26] G.E. Spangler, R.A. Miller, Int. J. Mass Spectrom. 214 (2002) 95.
[27] G.E. Spangler, Issues related to the drift theory for ion mobility spectrometry, in: Proceedings of the 2nd International Workshop on IMS, Que., Canada, August 1993.
[28] J. Urquijo, I. Alvarez, C. Cisneros, H. Martinez, Int. J. Mass Spectrom. Ion Process. 154 (1996) 25;
J.H. Whealton, J. Phys. B: Atom. Mol. Phys. 7 (1974) 1602.
[29] L.B. Jackson, Signals, Systems, and Transforms, Addison-Wesley, Reading, MA, 1991 (Chapter 2.3).
[30] G.E. Spangler, P.A. Lawless, Anal. Chem. 50 (1978) 290.
[31] D. Halliday, R. Resnick, Physics, Wiley, New York, 1962 (Chapter 28).
[32] X.R. Li, Probability, Random Signals, and Statistics, CRC Press, Boca Raton, FL, 1999 (Chapter 4).
[33] PCP, Inc., West Palm Beach, FL, A Subsidiary of Saes Getters S.p.A., Lainate, Italy.
[34] E.A. Mason, E.W. McDaniel, Transport Properties of Ions in Gases, Wiley, New York, 1988 (Chapter 1.1).
[35] J.M. Preston, L. Rajadhyax, J. Phys. Chem. 60 (1988) 31.
[36] K. Giles, E.P. Grimsrud, J. Phys. Chem. 97 (1993) 1318.
[37] K.E. Sahlstrom, W.B. Knighton, E.P. Grimsrud, J. Phys. Chem. 101 (1997) 1501.
[38] A.H. Lawrence, P. Neudorfl, J.A. Stone, Int. J. Mass Spectrom. 209 (2001) 185.
[39] S.B. Woo, J.H. Whealton, Phys. Rev. 180 (1969) 314.
[40] K. Iinuma, Can. J. Chem. 69 (1991) 1090.
[41] G.E. Spangler, Field Anal. Chem. Technol. 4 (5) (2000) 255.
[42] P. Kebarle, Ann. Rev. Phys. Chem. 28 (1977) 445.
[43] E.A. Mason, E.W. McDaniel, Transport Properties of Ions in Gases, Wiley, New York, 1988 (Chapter 5).
[44] E.A. Mason, H.W. Schamp, Ann. Phys. NY 4 (1958) 233.
[45] E.A. Mason, H. O'Hara, F.J. Smith, J. Phys. B: Atom. Mol. Phys. 5 (1972) 169.
[46] L.A. Viehland, S.L. Lin, E.A. Mason, J. Chem. Phys. 54 (1981) 341.
[47] P.L. Patterson, J. Chem. Phys. 56 (1972) 3943.
[48] (a) H.W. Ellis, R.Y. Pai, E.W. McDaniel, E.A. Mason, L.A. Viehland, Atom. Data Nucl. Data Tables 17 (1976) 177;
(b) H.W. Ellis, E.W. McDaniel, D.L. Albritton, L.A. Viehland, S.L. Lin, E.A. Mason, Atom. Data Nucl. Data Tables 22 (1978) 179;
(c) H.W. Ellis, M.G. Thackston, E.W. McDaniel, E.A. Mason, Atom. Data Nucl. Data Tables 31 (1984) 113;
(d) L.A. Viehland, E.A. Mason, Atom. Data Nucl. Data Tables 60 (1995) 37.
[49] S.H. Suck, D.E. Hagen, J.L. Kassner, L.E. Stoddard, J. Chem. Phys. 79 (1983) 4502.
[50] J.M. Mäkela, M. Riihelä, A. Ukkonen, V. Jokinen, J. Keskinen, J. Chem. Phys. 105 (1996) 1562.
[51] (a) Z. Karpas, Z. Berant, J. Phys. Chem. 93 (1989) 3021;
(b) Z. Karpas, Z. Berant, O. Shahal, J. Am. Chem. Soc. 111 (1989) 6015.
[52] E.W. McDaniel, Atomic Collisions: Electron & Photon Projectiles, Wiley, New York, 1989 (Chapter 3).
[53] G.E. Spangler, Field Anal. Chem. Technol. 4 (2000) 255.
[54] E.A. Mason, Ion mobility: its role in plasma chromatography, in: T.W. Carr (Ed.), Plasma Chromatography, Plenum Press, New York, 1984 (Chapter 2).
[55] J.H. Noggle, Physical Chemistry, Little, Brown & Co., Boston, 1984 (Chapter 1).
[56] A. Bondi, J. Phys. Chem. 68 (1964) 441.
[57] W.J. Lyman, W.F. Reehl, D.H. Rosenblatt, Handbook of Chemical Property Estimation Methods: Environmental Behavior of Organic Compounds, McGraw-Hill, New York, 1982 (Chapter 19).
[58] R.C. Reid, J.M. Prausnitz, T.K. Sherwood, The Properties of Gases and Liquids, 3rd Edition, McGraw-Hill, New York, 1977, p. 16.
[59] M. Abramowitz, I.A. Stegun, Handbook of Mathematical Functions, Dover, New York, 1965 (Section 7.5, Example 1).
[60] M. Abramowitz, I.A. Stegun, Handbook of Mathematical Functions, Dover, New York, 1965 (Formula 7.1.19).
[61] M. Abramowitz, I.A. Stegun, Handbook of Mathematical Functions, Dover, New York, 1965 (Formula 22.4.8).
[62] M. Abramowitz, I.A. Stegun, Handbook of Mathematical Functions, Dover, New York, 1965 (Formula 22.1.2 and Table 22.2).